Biomechan Model Mechanobiol (2008) 7:127–137
DOI 10.1007/s10237-007-0080-3

ORIGINAL PAPER

Non-linear viscoelastic behavior of abdominal aortic aneurysm thrombus

Evelyne A. van Dam · Susanne D. Dams · Gerrit W. M. Peters · Marcel C. M. Rutten · Geert Willem H. Schurink · Jaap Buth · Frans N. van de Vosse

Received: 2 October 2006 / Accepted: 17 February 2007 / Published online: 10 May 2007

Abstract The objective of this work was to determine the linear and non-linear viscoelastic behavior of abdominal aortic aneurysm thrombus and to study the changes in mechanical properties throughout the thickness of the thrombus. Samples are gathered from thrombi of seven patients. Linear viscoelastic data from oscillatory shear experiments show that the change of properties throughout the thrombus is different for each thrombus. Furthermore the variations found within one thrombus are of the same order of magnitude as the variation between patients. To study the non-linear regime, stress relaxation experiments are performed. To describe the phenomena observed experimentally, a non-linear multimode model is presented. The parameters for this model are obtained by fitting this model successfully to the experiments. The model cannot only describe the average stress response for all thrombus samples but also the highest and lowest stress responses. To determine the influence on the wall stress of the behavior observed the model proposed needs to implemented in the finite element wall stress analysis.

E. A. van Dam · S. D. Dams · M. C. M. Rutten (✉) · F. N. van de Vosse
Department of Biomedical Engineering, Technische Universiteit Eindhoven, PO box 513, WH4.120, 5600 MB, Eindhoven, The Netherlands
e-mail: m.c.m.rutten@tue.nl

G. W. M. Peters
Department of Mechanical Engineering, Technische Universiteit Eindhoven, Eindhoven, Netherlands

G. W. H. Schurink
Department of Vascular Surgery, University Hospital Maastricht, Maastricht, Netherlands

J. Buth
Department of Vascular Surgery, Catharina Hospital Eindhoven, Eindhoven, Netherlands

1 Introduction

Rupture of an abdominal aortic aneurysm (AAA) is a life threatening event, that can, when diagnosed in time, be prevented by either conventional or endovascular repair. Since these corrections are accompanied by mortality rates of 4.0 and 2.9%, respectively (Hua et al. 2005), a careful evaluation of the rupture risk versus the risk of surgical intervention is required. Currently, rupture risk prediction is based on the maximum diameter of the aneurysm. It has, however, been shown already that small aneurysms do rupture sometimes, while some large aneurysms have not ruptured yet, and therefore the diameter criterion alone may not be sufficient. Since the aneurysm wall ruptures when stress exceeds the strength of the vessel wall (Fillinger et al. 2003), stress analyses of the AAA vessel wall by means of a Finite Element Method (FEM), have become subject of several studies (di Martino et al. 1998; Fillinger et al. 2002; Inzoli et al. 1993; Mower et al. 1997; Raghavan et al. 2000; Thubrikar et al. 2001; Wang et al. 2002; Wolters et al. 2005). AAAs are lined with intraluminal laminated thrombus to a varying extent. The effect of the presence of thrombus on the wall stress has been studied on both idealized (di Martino et al. 1998; Inzoli et al. 1993; Mower et al. 1997) and patient specific geometries (di Martino and Vorp 2003; Wang et al. 2002). Thrombus is found to reduce and redistribute wall stress. The size of the effect is dependent on the geometry and the mechanical properties of the thrombus.

Thrombus is a fibrin structure infiltrated with blood cells, blood proteins and cellular debris (Falk 1992). Observation of thrombus (van Dam et al. 2006; Wang et al. 2001) reveals

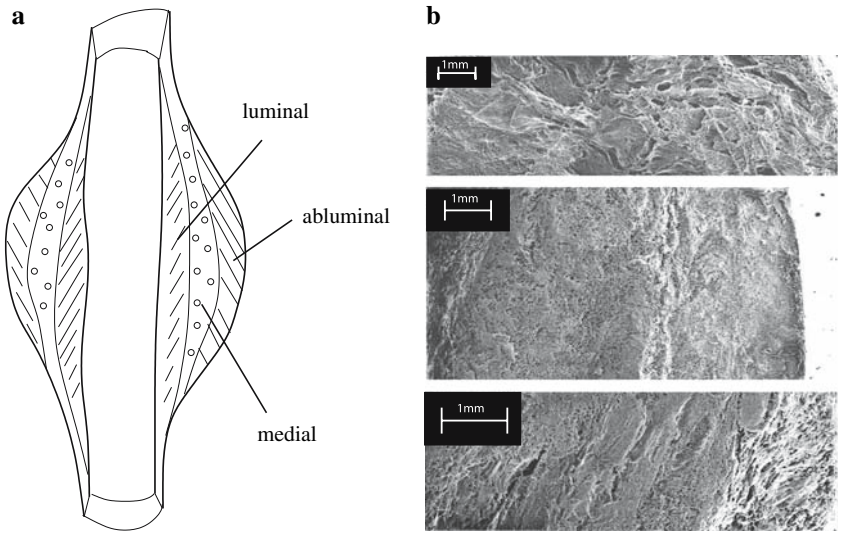

Fig. 1 Thrombus can be divided into luminal, medial and abluminal thrombus. In ESEM images of thrombus of three patients no large structural change can be found throughout the thrombus. At the left the luminal thrombus, at the right the abluminal thrombus

that three types of thrombus exist (Fig. 1a). New thrombus is formed at the luminal side and appears red. Fibrin fibers are clearly identifiable, and arranged into primary, thick fibrin bundles and a fine, secondary, cross linked structure. Attached to this thrombus is a more aged region, which appears white. Fibrin fibers in this regions have degenerated. In the abluminal region, the thrombus has aged most and all fibers appear degenerated, no structure can be recognized (Wang et al. 2001).

Figure 1b shows ESEM images, obtained in our lab, of the transversal plane through three different human AAA thrombi. The abluminal thrombus is at the right side of the image, luminal at the left side of the images. In the first thrombus, the local differences in structure are large. The structure is very dense in some positions, whereas it is very loose in others. The structure of the other two thrombi seems to be much more homogeneous, but still differences between areas can be pointed out. Wang et al related the mechanical properties of the luminal and medial thrombus to their structural state and reported a difference between the layers (Wang et al. 2001). The ESEM images in Fig. 1b, however, do not show clear distinction between the luminal, medial and abluminal layers, but do show large local variations. This may indicate that local variations can also occur in the mechanical properties.

The effects of local differences in structure were, however, neglected in the concerning wall stress analyses. The thrombus was modeled as an isotropic homogeneous material in all studies; the mechanical properties were either assumed (Inzoli et al. 1993; Mower et al. 1997) or were determined by fitting tensile testing data to a linear elastic model (di Martino et al. 1998) or to a two-parameter, hyper-elastic, isotropic and incompressible model (Wang et al. 2001, 2002). An ideal model for calculating AAA wall stresses would include loading with a dynamic pressure and applying a proper constitutive model that also incorporates the position dependent viscoelastic properties of the thrombus.

It has been shown in previous studies that rheological measurements yield reproducible results for linear viscoelastic behavior, which is valid for small strains up to 5% (Hinnen et al. 2007; van Dam et al. 2006). Large strains can, however, appear in thrombus (Vorp et al. 1996). When the change of shape of in vivo AAA's during systole was studied based on MR images inner, circumferential strains up to 15% were revealed. Since linear viscoelastic behavior is only applicable to small strains, the goal of this study is to determine the non-linear viscoelastic behavior of the thrombus and to study the changes in mechanical properties throughout the thickness of the thrombus caused by structural changes as described by Wang et al. (2001).

To achieve this goal, first a non-linear viscoelastic material model is presented that is able to capture the phenomena observed experimentally. To obtain the model parameter values, results of experiments in both the linear as the non-linear regime are needed. The changes in the linear behavior throughout the thickness of the thrombus, that may be caused by structural changes, will be shown. Although the oscillatory shear experiments were performed earlier (van Dam et al. 2006), they were repeated for a larger number of samples and the experimental methods were extended to the non-linear regime. Stress relaxation experiments are performed to obtain the non-linear model parameters.

2 Methods

2.1 Kinematics

The changes of volume and shape of an arbitrary solid material are described by the deformation gradient tensor

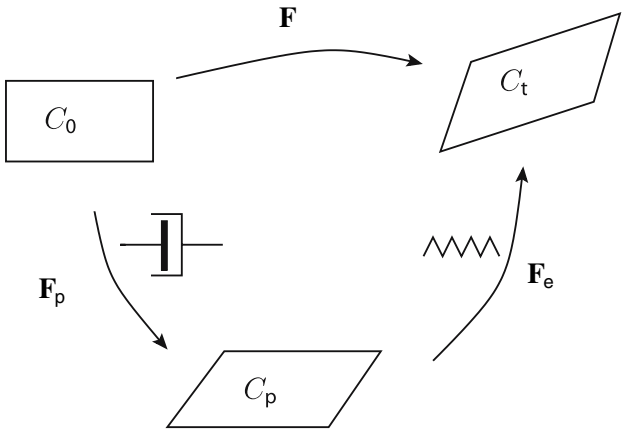

Fig. 2 The inelastic part of $\mathbf{F}$, $\mathbf{F}_p$ transforms the undeformed state C_0 to a relaxed stress-free configuration, C_p and is modeled by a dashpot. C_p is a fictitious state that would be recovered instantaneously when all loads were removed from the material element. The elastic part, $\mathbf{F}_e$, of $\mathbf{F}$ transforms the stress-free state C_p elastically into the deformed state C_t. This part is modeled by a spring

$\mathbf{F}$. $\mathbf{F}$ is split (Fig. 2) into an elastic part, $\mathbf{F}_e$, and an inelastic part $\mathbf{F}_p$:

$$\mathbf{dx} = \mathbf{F} \cdot \mathbf{dx}_0; \qquad \mathbf{F} = \mathbf{F}_e \cdot \mathbf{F}_p, \tag{1}$$

where $\mathbf{dx}_0$ represents a material line element in the undeformed state, C_0, and $\mathbf{dx}$ represents it in the deformed state, C_t. The inelastic part of $\mathbf{F}$, $\mathbf{F}_p$, transforms the undeformed state, C_0, to a relaxed stress-free configuration, C_p. This is a fictitious state that would be recovered instantaneously when all loads were removed from the material line-element. The elastic part, $\mathbf{F}_e$, of $\mathbf{F}$ transforms the stress-free state, C_p, elastically into the deformed state, C_t. Next, the elastic Finger tensor, $\mathbf{B}_e$, can be introduced:

$$\mathbf{B}_e = \mathbf{F}_e \cdot \mathbf{F}_e^{\mathrm{T}} \tag{2}$$

The velocity gradient tensor can be defined as

$$\mathbf{L} = \dot{\mathbf{F}} \cdot \mathbf{F}^{-1}. \tag{3}$$

Using (1) and (3) an additive decomposition of $\mathbf{L}$ is defined:

$$\begin{aligned} &\mathbf{L} = \mathbf{L}_e + \mathbf{L}_p, \\ &\mathbf{L}_e = \dot{\mathbf{F}}_e \cdot \mathbf{F}_e^{-1}, \quad \mathbf{L}_p = \mathbf{F}_e \cdot \dot{\mathbf{F}}_p \cdot \mathbf{F}_p^{-1} \cdot \mathbf{F}_e^{-1}. \end{aligned} \tag{4}$$

Both parts of the velocity gradient can be decomposed in:

$$\begin{aligned} &\mathbf{L}_e = \mathbf{D}_e + \mathbf{\Omega}_e, \quad \mathbf{D}_e = \frac{1}{2}(\mathbf{L}_e + \mathbf{L}_e^{\mathrm{T}}), \quad \mathbf{\Omega}_e = \frac{1}{2}(\mathbf{L}_e - \mathbf{L}_e^{\mathrm{T}}) \\ &\mathbf{L}_p = \mathbf{D}_p + \mathbf{\Omega}_p, \quad \mathbf{D}_p = \frac{1}{2}(\mathbf{L}_p + \mathbf{L}_p^{\mathrm{T}}), \quad \mathbf{\Omega}_p = \frac{1}{2}(\mathbf{L}_p - \mathbf{L}_p^{\mathrm{T}}) \end{aligned} \tag{5}$$

where $\mathbf{D}_e$ and $\mathbf{D}_p$ are the symmetric rate of deformation tensors and $\mathbf{\Omega}_e$ and $\mathbf{\Omega}_p$ are the skew-symmetric spin tensors. To obtain a unique fictitious stress free state, C_p, the inelastic deformation is assumed to occur spin free:

$$\mathbf{\Omega}_p = 0. \tag{6}$$

The elastic part of the deformation must then account for all rotations:

$$\mathbf{\Omega}_e = \mathbf{\Omega}. \tag{7}$$

2.2 The constitutive model

The constitutive model proposed is based on previous research on the viscoelastic properties of brain tissue (Hrapko et al. 2006).

Since thrombus can be assumed to be incompressible (Hinnen et al. 2007), the Cauchy stress can be split:

$$\boldsymbol{\sigma} = \boldsymbol{\sigma}^d + \boldsymbol{\sigma}^v, \tag{8}$$

where $\boldsymbol{\sigma}^v$ is the volumetric part, that only depends on the hydrostatic pressure ($p = -\frac{1}{3}\mathrm{tr}(\boldsymbol{\sigma})$), and $\boldsymbol{\sigma}^d = \boldsymbol{\sigma} - p\mathbf{I}$ is the deviatoric part. The latter part is decomposed into an elastic part, $\boldsymbol{\sigma}_0^d$ and into n viscoelastic modes (Fig. 3):

$$\boldsymbol{\sigma}^d = \boldsymbol{\sigma}_0^d + \sum_{i=1}^{n} \boldsymbol{\sigma}_i^d. \tag{9}$$

The elastic behavior of the viscoelastic modes is modeled as being Neo-Hookean:

$$\boldsymbol{\sigma}_i^d = G_i \mathbf{B}_{e,i}^d, \tag{10}$$

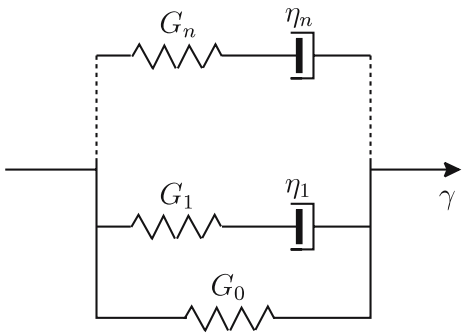

Fig. 3 A spring-dashpot model as a mechanical analog of the constitutive model. The springs G_1 through G_n and the dashpots in the viscoelastic modes are linear. The equilibrium mode is modeled by a non-linear spring G_0

where $B^d_{e,i}$ is the deviatoric part of the elastic Finger tensor $\mathbf{B}_e$ of mode i. The time dependent behavior of the viscoelastic modes is described by the inelastic rate of deformation, $\mathbf{D}_p$:

$$\mathbf{D}_{p,i} = \frac{\boldsymbol{\sigma}^d_i}{2\eta_i} \tag{11}$$

with $\eta_i = G_i \lambda_i$. This is equivalent to a Leonov model; a non-linear model that is fully characterized by the linear parameters G_i and λ_i only. In the limits of small strains this model reduces to a Maxwell model.

A non-linear equilibrium mode is added to the viscoelastic modes. This mode is described by a Mooney-Rivlin-type model, modified with a damping function:

$$\boldsymbol{\sigma}^d_0 = 2\frac{\partial W}{\partial I_1}\mathbf{B}^d - 2\frac{\partial W}{\partial I_2}(\mathbf{B}^{-1})^d, \tag{12}$$

with $W = W(I_1, I_2)$ the strain energy function, where $I_1$and I_2 are the first and second invariants of the Finger tensor:

$$I_1 = \mathrm{tr}(\mathbf{B}); \qquad I_2 = \frac{1}{2}[\mathrm{tr}(\mathbf{B})^2 - \mathrm{tr}(\mathbf{B}^2)]. \tag{13}$$

The shape of the partial derivatives of the strain energy function is chosen based on the non-linear strain-dependency of the equilibrated response as is observed in shear relaxation tests:

$$W = G_0\left\{-\frac{1-A}{C^2}[(Cx+1)\exp(-Cx) - 1] + \frac{1}{2}Ax^2\right\}, \tag{14}$$

with

$$x = \sqrt{bI_1 + (1-b)I_2 - 3} \tag{15}$$

and A, C and b material specific parameters. With this strain energy function, the constitutive relation for the equilibrium mode can be written as

$$\begin{aligned}\boldsymbol{\sigma}^d_0 = {} & G_0[(1-A)\exp(-C\sqrt{bI_1 + (1-b)I_2 - 3}) + A] \\ & \times[b\mathbf{B}^d - (1-b)(\mathbf{B}^{-1})^d].\end{aligned} \tag{16}$$

The parameter b distinguishes between the contribution of the first and second invariant of $\mathbf{B}$ to the strain energy and cannot be determined in shear experiments. This parameter is, in absence of other than shear experimental data, set to $b = 1$. Determination of b will be subject of future research by adding compression tests to the experimental methods. Equation (16) then can be simplified:

$$\boldsymbol{\sigma}^d_0 = G_0[(1-A)\exp(-C\sqrt{I_1 - 3}) + A]\mathbf{B}^d. \tag{17}$$

The constitutive model, (10), (11) and (17), describes the material behavior of the individual elements, i.e. the springs and dashpots. In each mode, the behavior of the springs is described as a function of the isochoric elastic Finger tensor $\mathbf{B}^d_{e,i}$, while the dashpots are described as a function of the inelastic deformation rate, $\mathbf{D}_{p,i}$. For numerical implementation, the kinematics is used to write the behavior in terms of the inelastic right Cauchy-Green tensor for each mode $\mathbf{C}_p$:

$$\mathbf{C}_p = \mathbf{F}^{\mathrm{T}}_p \cdot \mathbf{F}_p = \mathbf{F}^{\mathrm{T}} \cdot \mathbf{B}^{-1}_e \cdot \mathbf{F}. \tag{18}$$

Taking the time derivative of $\mathbf{C}_p$ and using the requirement of spin-free inelastic deformation, (6), provides an evolution equation for large rigid-body rotation and translation

$$\dot{\mathbf{C}}_p = 2\mathbf{C}_p \cdot \mathbf{F}^{-1} \cdot \mathbf{D}_p \cdot \mathbf{F}. \tag{19}$$

In the time integration procedure (Brands 2002), the evolution equation, $\dot{\mathbf{C}}_p$ is used to numerically update $\mathbf{C}_p$ (19) in the following way: At each new time increment the updated elastic Finger tensor follows from $\mathbf{F}$ at that time increment and (18): $\mathbf{B}_e = \mathbf{F}\cdot\mathbf{C}^{-1}_p\cdot\mathbf{F}^{\mathrm{T}}$. Application of $\mathbf{B}_e$ in constitutive equation (10) yields an updated $\boldsymbol{\sigma}^d_i$. Finally, the inelastic rate of deformation $\mathbf{D}_p$ is determined from (11) and the subsequently updated $\dot{\mathbf{C}}_p$, (19), serves as the basis for proceeding to the next step. The evolution equation, $\dot{\mathbf{C}}_p$, is insensitive for large-body rotations (Brands 2002) and is therefore used to to numerically update $\mathbf{C}_p$ (19).

The material parameters, G_0 to G_n, λ_1 to λ_n, A and C, are determined by fitting the proposed model to experimental data as will be described in the next section.

2.3 Determination of material parameters

2.3.1 Sample preparation

Thrombus tissue was obtained from seven patients undergoing elective surgical AAA repair. Because this material is discarded in the normal clinical setting and it is anonymized after the procedure, making tracing back to the patient impossible, informed consent was not required. The procedure was in conformity with the code of conduct for use of human material as stated by the Dutch federation of Biomedical Scientific Societies. Directly after harvesting of the tissue, it was stored in Phosphate Buffered Saline (PBS). The thickest part of the thrombus was selected for preparation of samples for mechanical testing. A vibratome (VS1000s, Leica microsystems, Germany) with a sapphire knife was used to cut a radially oriented stack of slices (Fig. 4), each with a thickness of 0.5 mm. For experiments performed on a plate plate configuration rheometer, the samples need to be

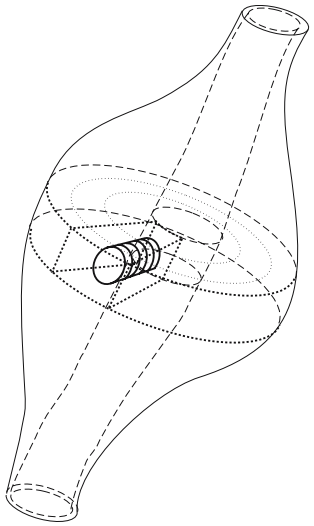

Fig. 4 Schematic view of the sample orientation

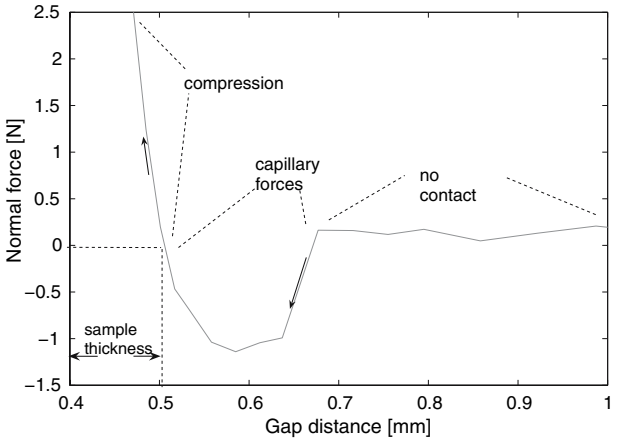

Fig. 5 Force Gap Test: The gap distance versus the normal force. When the gap distance is decreased, capillary forces will lead to a negative force. When the gap is decreased even further the force will rise through zero and the sample will be compressed. The sample thickness is taken equal to the smallest gap distance at which the normal force equals zero, in this case 0.5 mm

parallel. A cork drill with a diameter of 10 mm was used to cut a sample out of each slice. Since this sample preparation is time-consuming, measurements had to be postponed and samples were stored at −80°C. In a previous study it was verified that this storage did not influence the mechanical properties (van Dam et al. 2006). Before testing, the samples were thawed in a bath with lukewarm water.

2.3.2 Experimental setup

All small strain and large strain experiments were performed on a Rheometrics rotational rheometer (ARES, Advanced Expansion System) with parallel disk geometry in combination with a Peltier Environmental control and a fluid bath. All measurements were performed at 37°C in a PBS saturated humid environment.

To avoid compression to be applied during the shear experiments, the exact thickness of each sample was determined. The gap between the plates needs to be equal to this thickness. To this end, the upper plate is positioned above the sample and is then lowered with a constant velocity, while measuring the normal force. A typical representation of this procedure, called the force gap test, is given in Fig. 5, where the normal force is plotted as a function of the gap width during the force gap test. Samples are saturated with PBS, which will form a layer of liquid on top of the sample. When the upper plate nearly contacts the fluid, capillary effects will cause a negative normal force. When the plate is lowered further and reaches the sample top, the normal force will have increased again to zero. Evidently, the normal force will increase rapidly when the upper plate is lowered even further and compresses the sample.

2.3.3 Small strain experiments

For small strains, the non-linear viscoelastic model proposed in the previous paragraphs, reduces to a multimode Maxwell model. A n-mode Maxwell model is fully determined by the relaxation time λ_i and moduli $G_i (i = 1, \ldots, n)$ and can be presented in terms of the storage modulus G' and the loss modulus G'',

$$G' = G_0 + \sum_{i=1}^{n} G_i \frac{\lambda_i^2 \omega^2}{1 + \lambda_i^2 \omega^2}, \quad G'' = \sum_{i=1}^{n} G_i \frac{\lambda_i \omega}{1 + \lambda_i^2 \omega^2}, \tag{20}$$

where λ_i and G_i are a set of the relaxation time and shear modulus for the ith mode. For a given number of modes the values for G and λ can be acquired by a dynamic frequency sweep test (DFST). In a DFST, harmonic oscillations with a varying frequency at a constant strain are applied. DFST's were performed with a frequency range of 1 rad/s (0.16 Hz) to 100 rad/s (16 Hz) and a constant strain of 3%, which is within the linear viscoelastic regime of the thrombus (van Dam et al. 2006). The applicability of these small shear experiments was shown in previous work (van Dam et al. 2006). In this study, new samples were used to determine the non-linear parameters and to obtain complete datasets these new samples were also tested in the small strain regime. The obtained G' and G'' were used to the study the variations within and between thrombi. The original position within the thrombus of each slice plotted against the G' and G'' provide information about the changes of the viscoelastic properties throughout the thrombus. To obtain the differences between thrombi, the mean and standard deviation of G' per thrombus were used. To obtain the general model parameters λ_1 through λ_n

and G_0 through G_n, all G' and G'' curves were averaged. Equation (20) was fitted to these mean G' and G'' curves, with $n = 3$, using a least squares estimation algorithm.

2.3.4 Large strain experiments

To determine the model parameters of the non-linear material model described in the previous section, oscillatory experiments can be used. These experiments should then be done at a certain number of frequencies. When, however, stress relaxation experiments are performed information is gathered about all frequencies present within the limits of the experimental setup. During the stress relaxation experiments, a theoretical step in strain is imposed on the sample. Since this is not possible in reality, stress relaxation strain ramps with increasing magnitude (1, 5, 10, 15 and 20%) are imposed with a strain rate of $1\,s^{-1}$ (Fig. 6). Strain is kept constant thereafter for a loading time of 10s ($\omega < 2\pi/10s \approx 0.5$). After this loading phase the strain is released and the sample is left to recover at zero strain for ten times the loading time. Besides the facts that we explore the nonlinear regime and a range of frequencies, these experiments also provide information about reproducibility and the relaxation behavior.

The evolution equation (19) was implemented numerically as described in Sect. 2.2 and the model then was fitted to the results from the stress relaxation experiments using a least squares estimation algorithm. The stress responses to the applied strain (Fig. 6) of all samples were averaged and the resulting mean stress response was used in the fitting procedure.

Moduli, G_1 through G_3 and relaxation times λ_1 through λ_3, as determined for the linear regime are assumed to be true for the non-linear case as well. Relaxation, however, continues up to 10 s, but the small strain experiments do not include such low frequencies. The large relaxation time that is expected from the stress-relaxation experiment can therefore not be found by fitting it solely to the small strain results. A fourth viscoelastic mode, with G_4 and λ_4, is therefore introduced. Addition of a viscoelastic mode will influence the total G' and G'' (according to (20)) and therefore G_0 is fitted again. Since G_0 also influences the nonlinear regime (according to (17)), the fitting routine simultaneously evaluates the parameters for small strains, (20), and large strains (19) with the objective function:

$$\epsilon = \frac{1}{n}\sum_{i=1}^{n}\left(\frac{(G'_{\mathrm{mod}}(i)-G'_{\mathrm{exp}}(i))^2}{G'^2_{\mathrm{exp}}(i)} + \frac{(G''_{\mathrm{mod}}(i)-G''_{\mathrm{exp}}(i))^2}{G''^2_{\mathrm{exp}}(i)}\right) + \frac{1}{m}\sum_{j=1}^{m}(\sigma_{\mathrm{mod}}(j) - \sigma_{\mathrm{exp}}(j))^2 \tag{21}$$

where G'_{mod}, G''_{mod} and σ_{mod} are the modeled values and G'_{exp}, G''_{exp} and σ_{exp} the experimental values. G' and G'' are measured (and modeled) at n points, σ is measured at m points. In this objective function errors between the modeled and measured linear data are normalized to experimental values, whereas the non-linear error is not normalized. Normalization of the non-linear error to the measured value is impossible because at some measurements points it will lead to divide-by-zero.

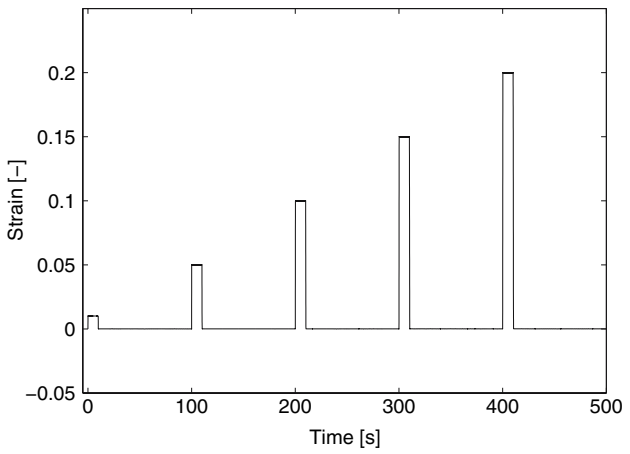

Fig. 6 Stress relaxation experiments: strain ramps with increasing magnitude are imposed

3 Results

3.1 Small strain experiments

To determine the thickness of each sample the force gap test was performed before further testing. The thickness of the samples varied between 0.4 and 0.6 mm.

The frequency sweep results show the variations of material properties within and between patients. G' and G'' at 10 rad/s are plotted against the relative position of the sample in the thrombus (Fig. 7). Position 0 corresponds to the abluminal side, while position 1 indicates the luminal side. The G' values are all in the same order of magnitude and are within a range of 1.7 ± 1.3 kPa. When studying the change of G' throughout the thickness of each thrombus no similar trend for all patients can be found. The results for G'' are similar: all values are in the same order of magnitude (0.2 ± 0.1 kPa) and no similar trends can be found throughout the thrombus for the different patients. G' of patient 1, e.g., increases towards the abluminal side while G' of patient 2 decreases.

Figure 8 depicts the mean and standard deviation of G' and G'' over all samples separately. The values G' and G'' do not differ significantly between patients.

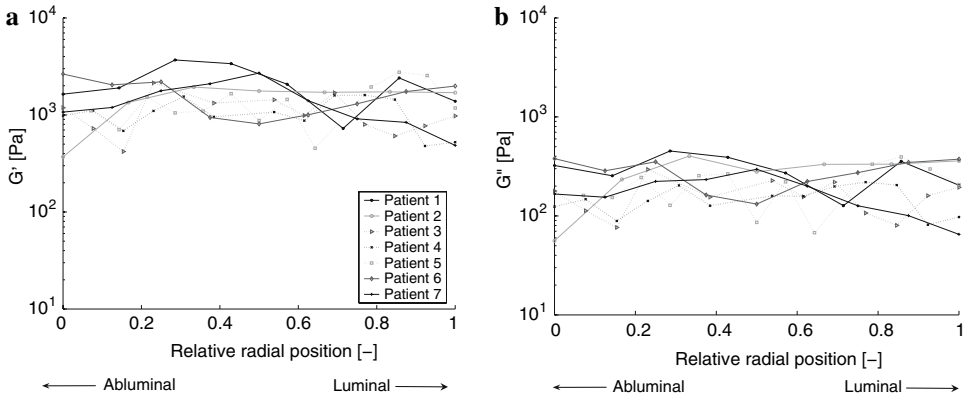

Fig. 7 G' (**a**) and G'' (**b**) at 10 rad/s versus the relative position of each sample in the thrombus: 0 indicates the abluminal side, 1 indicates the luminal side of the thrombus

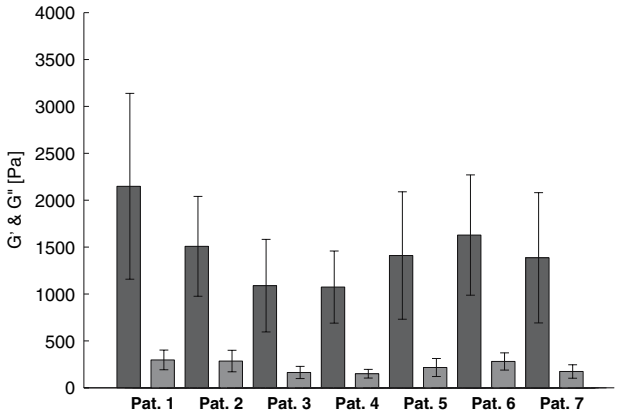

Fig. 8 The mean and standard deviation of G' and G'' at 10rad/s of all samples of each patient

The mean and standard deviation of all samples are given versus the frequency in Fig. 9. G' increases with frequency for all samples in a similar way. A Maxwell model with three viscoelastic modes and an equilibrium mode was fitted to the mean of all samples. The values for λ_i and G_i are given in Table 1, the resulting G' and G'' are plotted in Fig. 9. Both fitted G' and G'' are well within the standard deviation of the measured values and the multimode Maxwell model is therefore assumed to describe the linear material behavior in a satisfying way.

3.2 Large strain experiments

To obtain the parameters for the large strain regime, the stress relaxation experiments as described in Sect. 2.3.4 have been performed. The mean stress response of all samples has been used to obtain the model parameters.

In Fig. 10 a the mean stress responses for the 1, 5, 10, 15 and 20% strain are given (from bottom to top, respectively). Datapoints in the loading phase and the relaxation were used simultaneous to fit to the model. In the unloading phase too few datapoints were gathered, due to experimental limitations, to determine material properties.

In Fig. 10b, the same experimental data are presented as in Fig. 10a as a stress-strain curve. It can be seen that the model can describe the behavior in the loading and relaxation phase

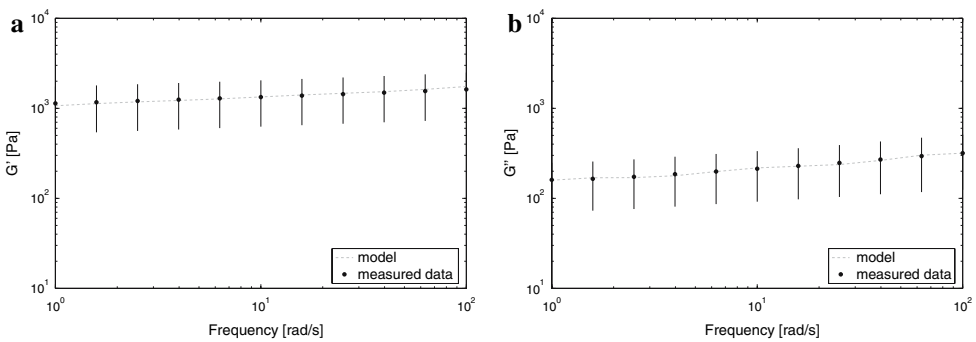

Fig. 9 Mean G' (**a**) and G'' (**b**) with the standard deviation over all samples. The mean value was fitted to a multimode Maxwell model

Table 1 Linear model parameters that describe the average G' and G''

G_0 (Pa)	G_1 (Pa)	G_2 (Pa)	G_3 (Pa)	λ_1 (s)	λ_2 (s)	λ_3 (s)
9.5×10^2	5.7×10^2	2.7×10^2	2.6×10^2	9.5×10^{-3}	9.6×10^{-2}	9.1×10^{-1}

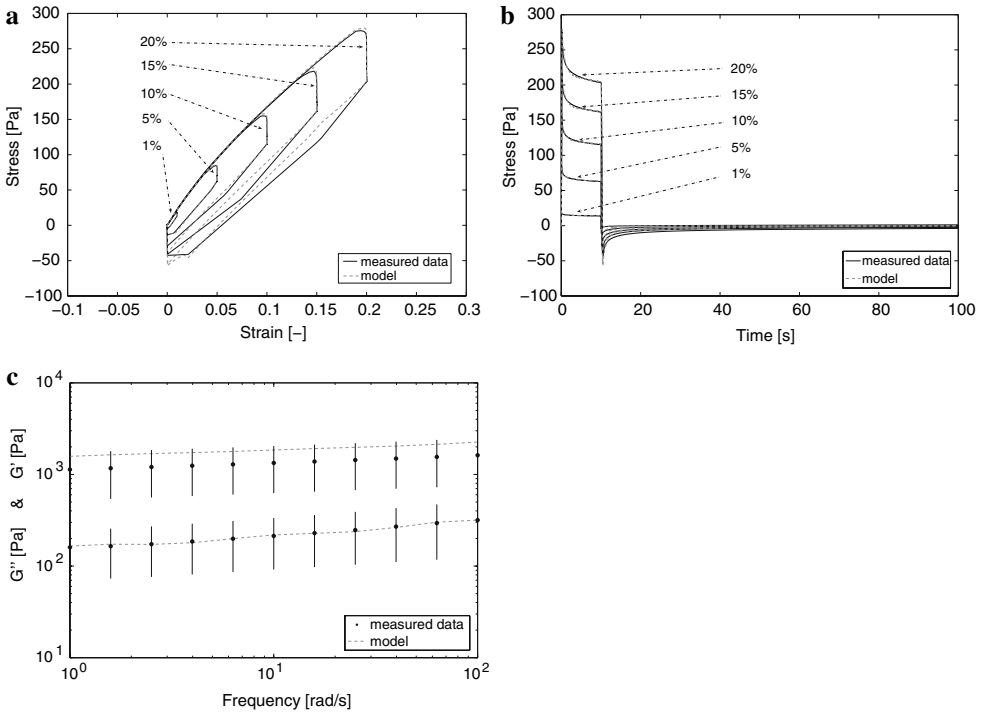

Fig. 10 Stress strain relation (**a**), the stress relaxation (**b**) and the linear parameters, G' and G'' (**c**), for the mean response together with the model description

rather good, however, the unloading phase is not described very well. The predicted relaxation is faster than the measured relaxation. Since a fourth viscoelastic mode is added and G_0 is estimated again, the values for G' and G'' have changed. In Fig. 10c, the mean and standard deviation of G' and G'' are shown together with the newly calculated value for G' and G'' according to (20). G' is overestimated after fitting the stress relaxation data, but is still within the standard deviation of the measured data.

4 Discussion

In this work the nonlinear viscoelastic properties of thrombus are studied. In previous research we did show that rheometry is a useful method to determine linear viscoelastic properties (van Dam et al. 2006). Since thrombus experiences large strains in vivo, the characterization of the material behavior has been extended to the non-linear regime. A non-linear multimode model to describe the viscoelastic behavior of the thrombus is chosen. This model consists of a number of non-linear viscoelastic modes, described by linear viscoelastic parameters G_i and λ_i only, and a non-linear equilibrium mode, described by a non-linear spring. The linear viscoelastic modes and the non-linear equilibrium mode were based on experimental data. If it is assumed that the loading time is long enough for the sample to relax completely, the coefficient in (17) can be taken as the last response before the load is released (Fig. 11a). If this coefficient is extracted for each strain and plotted against the strain, it is clear that it is decreasing with increasing strain (Fig. 11b). Thus, it is strain dependent in a non-linear way. When the response for each

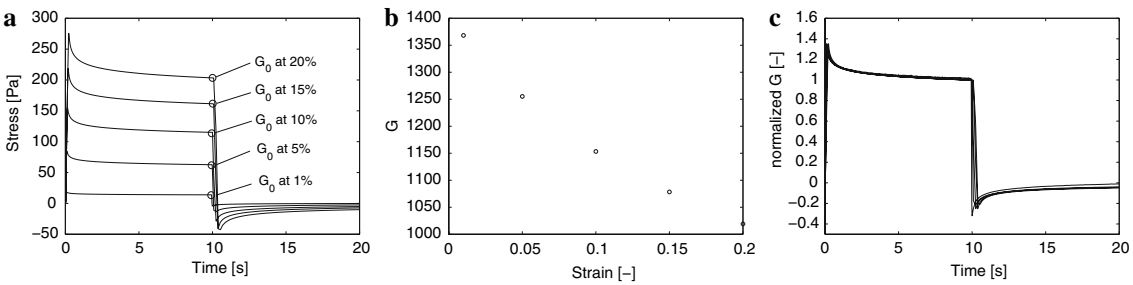

Fig. 11 When the coefficient of (17) is extracted from the stress relaxation responses (**a**), and plotted against the strain ($G = G_0 f(I_1)$) it can be seen that it is strain dependent (**b**) in a nonlinear way. When the stress responses are normalized to strain amplitude and the accompanying value for the coefficient, it is clear that the relaxation is linear dependent on the strain (**c**)

strain amplitude is normalized to the strain and the accompanying value for the coefficient of (17), it can be seen that the shape of the responses is equal for all strains (Fig. 11c). The relaxation behavior is strain dependent in a linear way. Therefore, linear springs and dashpots were chosen for the viscoelastic modes, whereas the equilibrium mode is described by a non-linear spring.

To obtain the linear model parameters, shear experiments in the linear strain regime were performed on thrombi from seven patients. As has been described earlier (van Dam et al. 2006) samples cannot be gathered from all parts of the thrombus. The tissue at the abluminal side of the thrombus is too degenerated to cut samples from. The abluminal thrombus is, however, responsible for the attachment of the thrombus to the wall. The nature of the thrombus-vessel wall contact is unclear to the authors, and will be a subject of further research. When studying the change of G' and G'' throughout the thickness of the thrombus, each thrombus shows it own curve. No general curve can be recognized that describes a gradual change of material properties throughout all different thrombi. Values found are all in the same order of magnitude. The mean value for G' and G'' does not differ significantly between patients.

Values for G' and G'' we have reported in earlier work (van Dam et al. 2006), were approximately three times higher than reported in this study. A possible reason for this is the use of a moisture chamber in this study. Dehydration of the sample could lead to altered mechanical properties. Hinnen et al. (2007) performed dynamic mechanical experiments on thrombus in the linear regime. They reported mean G' and G'' of 35 and 8 kPa, which is an order of magnitude higher than the values reported in this work. The results by Hinnen et al., may be influenced by their experimental method which included glueing of the sample.

Responses in the large strain regime have been studied by performing stress relaxation experiments. Since the loading phases of all curves, with increasing strain, overlap well, it can be concluded that the samples were not damaged during the experiments. Mechanical damage would have led to an immediate change in the response. To describe the behavior, model parameters were obtained from the experimental data. The fitting procedure resulted in a unique parameter set as long as the initial guesses for G and λ are within the same range as the experiments.

All the non-linear parameters play a specific role. Parameter b allows for weighting between the invariants I_1 and I_2 and, therefore, distinguish between the non-linear behavior in shear and extension ($I_1 = I_2$. in shear, $I_1 > I_2$ in extension). The non-linear behavior is fully captured with the parameters A and C. The strength of the non-linearity is described by C, while A weights the non-linearity with the linear part. Without going into detail (because it is outside the scope of the paper) we would like to mention that most parameters, linear and non-linear, are not only weakly correlated except for those that determine the level of the stress, i.e. A, G_0 and G_4 (the mode with the highest relaxation time and thus the most elastic mode).

Convexity is a restriction of the strain energy density function, W, that prevents numerical instability (Holzapfel et al. 2000). Convexity is, however, suggested to be too restrictive and furthermore a disagreement between experimental findings and convexity was reported (Bilgili 2004). Therefore, convexity is not taken into account in this work.

It has been shown that the mean response of all samples can be described by the non-linear multimode model, as described in Sect. 2.2, in a satisfying way. Whereas the stress relaxation is described very well, G' is overestimated by the model. This is the result of the objective function in which the non-linear error is weighted heavier than the non-linear error because of absence of normalization of the non-linear error. The overestimation can be prevented by applying normalization of the non-linear error to the mean value of the non-linear experimental data. The objective function then changes to:

$$\epsilon = \frac{1}{n}\sum_{i=1}^{n}\left(\frac{(G'_{\mathrm{mod}}(i) - G'_{\mathrm{exp}}(i))^2}{G'^2_{\mathrm{exp}}(i)} + \frac{(G''_{\mathrm{mod}}(i) - G''_{\mathrm{exp}}(i))^2}{G''^2_{\mathrm{exp}}(i)}\right) + \frac{1}{m}\sum_{j=1}^{m}\frac{(\sigma_{\mathrm{mod}}(j) - \sigma_{\mathrm{exp}}(j))^2}{\overline{\sigma_{\mathrm{exp}}}^2} \tag{22}$$

Figure 12 depicts the results of such a model fit. The description of G' has indeed improved, but the relaxation is now described poorly. When this model is to be implemented in a finite element model, the model parameters as described in the results section can best be chosen. A model for describing relaxation and stress-strain relation well is more relevant in the physiological situation than a model describing G' and G'' well.

The model parameters have been obtained for the mean response of all samples. Thrombi whose response level is extremely high or low may, however, have a pronounced influence on rupture risk prediction using finite element stress analysis. Therefore, the highest and lowest stress response were fitted to the model proposed. The measured relaxation and the fitted model for these samples is depicted in Fig. 13. It can be seen that the model can describe these outliers well. The model parameters for these extreme experimental results and the mean response are given in Table 2. It is found that G_0 is an important parameter in describing the behavior. The non-linear parameters C are all of the same order of magnitude. The variation in parameter A cannot clearly be related to either a high or low response. In the model used the

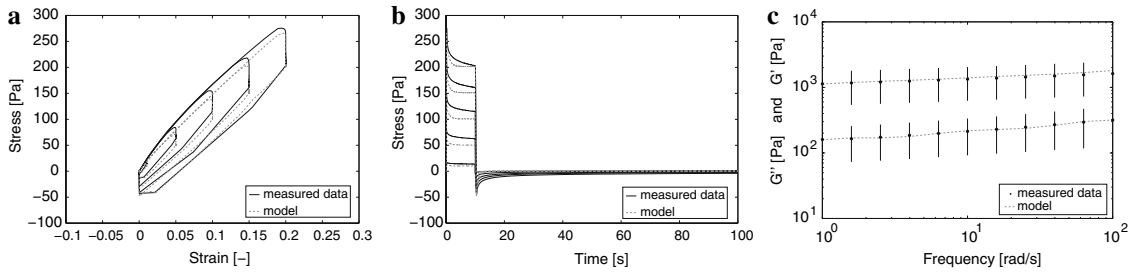

Fig. 12 Stress strain relation (**a**), the stress relaxation (**b**) and the linear parameters, G' and G'', for the mean response together with the model description. G' and G'' were weighted heavily in the fitting procedure

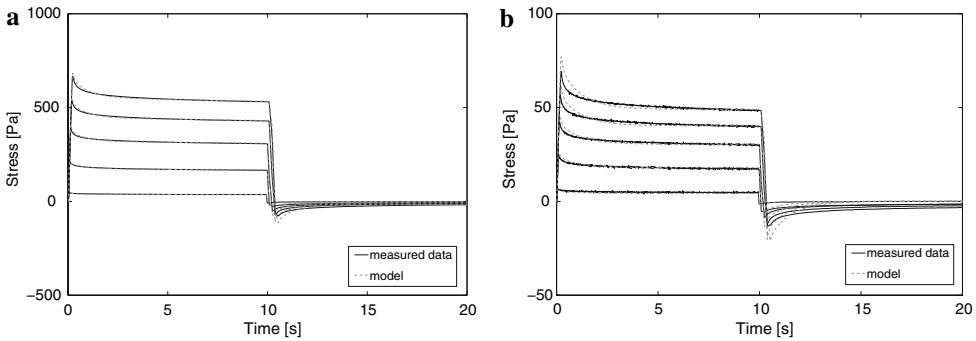

Fig. 13 The stress relaxation as measured together with the model description for the samples with the largest (**a**) and smallest (**b**) response

Table 2 Model parameters that describe mean response and the highest and lowest stress response

	Mean		Highest		Lowest	
Mode	G (Pa)	λ (s)	G (Pa)	λ (s)	G (Pa)	λ (s)
1	5.7×10^2	9.5×10^{-3}	1.1×10^3	1.0×10^{-2}	1.6×10^2	1.0×10^{-2}
2	2.7×10^2	9.6×10^{-2}	5.6×10^2	9.3×10^{-2}	9.7×10^1	1.0×10^{-1}
3	2.6×10^2	9.1×10^{-1}	5.3×10^2	8.7×10^{-1}	$1.1 \cdot 10^2$	1.1×10^0
4	1.7×10^2	2.8×10^1	1.1×10^3	1.1×10^2	$1.2 \cdot 10^{-9}$	1.2×10^2
G_0 (Pa)	1.3×10^3		2.7×10^3		4.4×10^2	
A (–)	5.7×10^{-1}		2.8×10^{-2}		4.6×10^{-1}	
C (–)	5.8×10^0		2.4×10^0		8.7×10^0	

parameter b is set to 1. Experiments other than shear experiments, such as compression tests, are necessary to be able to determine b. Since G' seems to be the major player in describing the thrombus behavior, only small differences are expected to be found for b. It would, however, be an interesting subject for further research.

The influence of the non-linear viscoelastic behavior can be studied by implementing the material model into finite element AAA stress calculations (Wolters et al. 2005). Although the moduli found are very low, the viscoelastic behavior may play a role in the attenuation of pressure waves traveling through the arterial system. When implementing the parameters found for the highest and lowest stress response leads to large variations in wall stress and its distribution, a method has to be developed to obtain the mechanical properties of thrombus in a patient-specific way. When the resulting variations in wall stress, however, are small, one may assume that all thrombi may be described with the same parameter set.

Wang et al. (2001) related the mechanical properties of luminal and medial thrombus to the structural state of the tissue. To study the relation between mechanical properties and structure of the tissue, ESEM images were also included in this work (Fig. 1b). On a global scale structural changes can be seen, but these differences cannot be found consistently in the material behavior. Local differences in structure could

lead to the local effects in properties that we found. The structure seen in ESEM images and the mechanical properties of samples taken from an adjacent slice of thrombus cannot be related directly. This would probably require ESEM images of each rheological sample.

5 Conclusion

From experimental data it is concluded that the change of properties throughout the thrombus is different for each thrombus. The variations found within one thrombus are of the same order of magnitude as the variation between patients. This suggests that the same material parameters may be used to describe all thrombi.

The multimode viscoelastic model proposed can be used to describe the linear and the non-linear viscoelastic properties of intraluminal thrombus. The parameters can be obtained successfully by fitting it to the experimental data. The model cannot only describe the average stress response but also the highest and lowest stress responses. This may play an important role in rupture risk prediction using finite element stress analysis and implementation of the model is needed to determine the influence on the wall stress of responses found.

References

Bilgili E (2004) Restricting the hyperelastic models for elastomers based on some thermodynamical, mechanical, and empirical criteria. J Elastom Plast, 36:159–175

Brands DWA (2002) Predicting brain mechanics during closed head impact -numerical and constitutive aspects-. PhD thesis, Technische Universiteit Eindhoven

di Martino ES, Mantero S, Inzoli F, Melissano G, Astore D, Chiesa R, Fumero R (1998) Biomechanics of abdominal aortic aneurysm in the presence of endoluminal thrombus: experiment characterisation and structural static computational analysis. Eur J Vasc Endovasc Surg 15:290–299

di Martino ES, Vorp DA (2003) Effect of variation in intraluminal thrombus constitutive properties on abdominal aortic aneurysm wall stress. Ann of Biomed Eng 31:804–809

Falk E (1992) Dynamics in thrombus formation. Ann New York Acad Sci pp 205–223

Fillinger MF, Raghavan ML, Marra SP, Cronenwett JL, Kennedy FE (2002) In vivo analaysis of mechanical wall stress and abdominal aortic aneurysm rupture risk. J Vasc Surg 36:589–597

Fillinger MF, Marra SP, Raghavan ML, Kennedy FE (2003) Prediction of rupture risk in abdominal aortic aneurysm during observation: wall stress versus diameter. J Vasc Surg 37(4):724–732

Hinnen JW, Rixen DJ, Koning OHJ, van Bockel JH, Hamming JF (2007) Development of fibrinous thrombus analogue for in-vitro abdominal aortic aneurysm studies. J Biomech 40(2):289–295

Holzapfel GA, Gasser TC, Ogden RW (2000) A new consitutive framework for arterial wall mechanics and a comparitive study of material models. J Elast 61:1–48

Hrapko M, van Dommelen JAW, Peters GWM, Wismans JSHM (2006) The mechanical behaviour of brain tissue: large strain response and constitutive modelling. Biorheology 43(5):623–636

Hua HT, Cambria RP, Chuang SK, Stoner MC, Kwolek CJ, Rowell KS, Khuri SF, Henderson WG, Brewster DC, Abbott WM (2005) Early outcomes of endovascular versus open abdominal aortic aneurysm repair in the national surgical quality improvement program-private sector (nsqip-ps).J Vasc Surg 41:382–389

Inzoli F, Boschetti F, Zappa M, Longo T, Fumero R (1993) Biomechanical factors in abdominal aortic aneurysm rupture. Eur J Vasc Endovasc Surg 7:667–674

Mower WR, Quinones WJ, Gambhir SS (1997) Effect of intraluminal thrombus on aortic aneurysm wall stress. J Vasc Surg 26(4):602–608

Raghavan ML, Vorp DA, Federle MP, Makaroun MS, Webster MW (2000) Wall stress distribution on three-dimensionally reconstructed models of human abdominal aortic aneurysm. J Vasc Surg 31(4):760–769

Thubrikar MJ, Al-Soudi J, Robicsek F (2001) Wall stress studies of abdominal aortic aneurysm in a clinical model. Ann Vasc Surg 15:355–366

van Dam EA, Dams SD, Peters GWM, Rutten MCM, Schurink GWH, Buth J, van de Vosse FN (2006) Determination of linear viscoelastic behavior of abdominal aortic aneurysm thrombus. Biorheology, 43(6):695–707

Vorp DA, Mandarino WA, Webster MW, Gorscan III J (1996) Potential influence of intraluminal thrombus on abdominal aortic aneurysm as assessed by a new non-invasive method. Cardiovasc Surg 4(6):732–739

Wang DHJ, Makaroun MS, Webster MW, Vorp DA (2001) Mechanical properties and microstructure of intraluminal thrombus from abdominal aortic aneurysm. J Biomech Eng 123:536–539

Wang DHJ, Makaroun MS, Webster MW, Vorp DA (2002) Effect of intraluminal thrombus on wall stress in patient-specific models of abdominal aortic aneurysm. J Vasc Surg 36:598–604

Wolters BJBM, Rutten MCM, Schurink GWH, Kose U, de Hart J, van de Vosse FN (2005) A patient-specific computational model of fluid-structure interaction in abdominal aortic aneurysms. Med Eng Phys 27:871–883